International Journal of Refrigeration 155 (2023) 47–57

Contents lists available at ScienceDirect

International Journal of Refrigeration

journal homepage: www.elsevier.com/locate/ijrefrig

Thermal-hydraulic characterization of R513A during flow boiling inside a 6.0 mm horizontal tube, comparison with R134a and development of a new correlation

Caractérisation thermohydraulique du R513A lors de l'ébullition en écoulement à l'intérieur d'un tube horizontal de 60 mm, comparaison avec le R134a et développement d'une nouvelle corrélation

A.W. Mauro *, F. Pelella, L. Viscito

Department of Industrial Engineering, Università degli Studi di Napoli – Federico II, P.le Tecchio 80, 80125 Naples, Italy

ARTICLE INFO

Keywords:
R513A
Low-GWP refrigerants
Flow boiling
Two-phase pressure drop
Assessment of correlations
Mots clés:
R513A
Frigorigènes à faible PRP
Ébullition en écoulement
Chute de pression diphasique
Évaluation des corrélations

ABSTRACT

This paper presents two-phase heat transfer coefficient and pressure drop data of refrigerant R513A, a new azeotropic mixture conceived as possible alternative to R134a for medium temperature small-size refrigeration systems. All the experiments were performed in a commercial horizontal stainless-steel tube having an internal diameter of 6.0 mm and an outer diameter of 8.0 mm. The channel heating was obtained through DC current and Joule effect. The effect of the main operating parameters in terms of mass flux (from 150 to 500 kg/m^{2}s), heat flux (from 5.0 to 40 kW/m^2), saturation temperature (from 30 to 50 °C) and vapor quality (from the onset of boiling up to the dry-out occurrence) was analyzed and discussed for the heat transfer coefficient values, finding that both convective and nucleate boiling were significant contributions. The same ranges of mass flux and saturation temperature were also applied to frictional pressure gradient trends with vapor quality, taken in adiabatic conditions. The thermo-hydraulic performances were then compared with those of R134a, obtaining lower heat transfer coefficients and very similar pressure gradients. Finally, the collected experiments were assessed with values predicted from the most quoted correlations available in literature. A new composite method for nucleate-dominant or convective-dominant mechanisms was proposed for the evaluation of the heat transfer coefficient, with a mean absolute error of 25.3%, whereas the frictional pressure gradient values were well predicted with the Friedel correlation, that provides a mean absolute error of 13.8%.

1. Introduction

The anthropic contribution to the global warming is a well-known issue, becoming increasingly discussed in the latest years (Stocker, 2013). The undesired rise of the Earth temperature has been in fact related to the huge amount of greenhouse gases released in the atmosphere and will probably increase in the developing countries all over the world (Ritchie and Roser, 2020). Among several fields, vapor compression refrigeration systems provide a substantial contribution, according to (Choi et al., 2017; Abas et al., 2018), mostly due to the use of high Global Warming Potential (GWP) hydrofluorocarbon (HFC) refrigerants that can be accidentally released during dismission or with leakages and soft faults (Pelella et al., 2022).

R404A, R134a and R410A are still the most used HFC refrigerants in the sectors of refrigeration and air conditioning, depending on the temperature levels. Particularly, R134a is the most common fluid in medium temperature applications of developed countries, including domestic and industrial air conditioning, automotive air conditioning and centrifugal chillers. According to the EU Regulation 517/2014 (The European Parliament and the Council of the European Union 2014) this substance is already banned since 2015 in domestic refrigerators and freezers, and since 2022 from commercial systems. Other sectors (commercial stationary refrigeration equipment and primary circuit of

* Corresponding author.
E-mail address: wmauro@unina.it (A.W. Mauro).

https://doi.org/10.1016/j.ijrefrig.2023.08.018
Received 28 July 2023; Received in revised form 9 August 2023; Accepted 29 August 2023
Available online 30 August 2023

Nomenclature

Roman

c	specific heat [J kg^{-1} K^{-1}]
D	outer diameter [m]
d	inner diameter [m]
E	enhancement factor [-]
g	acceleration of gravity [m s^{-2}]
G	mass flux [$kg{\cdot}m^{-2}{\cdot}s^{-1}$]
h	heat transfer coefficient [$W{\cdot}m^{-2}{\cdot}K^{-1}$]
i	specific enthalpy [$J{\cdot}kg^{-1}$]
I	current [A]
L	heated length [m]
$\dot{m}$	mass flow rate [$kg{\cdot}s^{-1}$]
M	molecular mass [kg $kmol^{-1}$]
p	pressure [Pa]
$\dot{Q}$	heat power [W]
q	heat flux [$W{\cdot}m^{-2}$]
S	suppression factor [-]
T	temperature [K]
V	voltage [V]
x	vapor quality [-]
z	position on the test section [m]

Greek

$\delta_{\pm 30\%}$	percentage of data points falling into $a \pm 30\%$ error band percentage of data points falling into $a \pm 30\%$ error band%
Δ	variation
ε	roughness [μm]
λ	thermal conductivity [$W{\cdot}m^{-1}{\cdot}K^{-1}$]
μ	dynamic viscosity [Pa s]
ρ	density [kg m^{-3}]
σ	surface tension [N m^{-1}]

Subscripts

c	related to the C measuring point
CB	convective boiling
exp	experimental
fr	friction
in	inlet
L	liquid
LO	liquid only
LV	liquid-to-vapor
m, mean	mean
NB	nucleate boiling
out	outlet
preh	preheater
red	reduced
sat	saturation
th	related to the thermocouple measurement
TS	test section
tube	related to the tube
V	vapor
VO	vapor only
wall	related to wall

Statistical parameters

$ER = \frac{h_{pred}-h_{exp}}{h_{exp}} \cdot 100$ Error in prediction

$MAPE = \frac{1}{n}\sum_i |ER_i|$ Mean Absolute Percentage Error

$MRPE = \frac{1}{n}\sum_i ER_i$ Mean Relative Percentage Error

Acronyms

GWP	Global Warming Potential
HFC	Hydrofluorocarbon
HFO	Hydrofluoroolefin
ODP	Ozone Depletion Potential

Non-dimensional numbers

Boiling number $Bo = \frac{q}{G\Delta i_{LV}}$

Bond number $Bd = \frac{g(\rho_L-\rho_V)d^2}{\sigma}$

Confinement number $Co = Bd^{-0.5}$

Froude vapor number $Fr_V = \frac{xG}{\sqrt{\rho_V \cdot (\rho_L-\rho_V) g d}}$

Martinelli parameter $X_{tt} = \left(\frac{1-x}{x}\right)^{0.9} \cdot \left(\frac{\rho_V}{\rho_L}\right)^{0.5} \cdot \left(\frac{\mu_L}{\mu_V}\right)^{0.1}$

Prandtl number $Pr = \frac{c}{\mu\lambda}$

Reynolds number $Re = \frac{Gd}{\mu}$

Weber number $We = \frac{G^2 d}{\rho\sigma}$

cascade systems) still may employ R134a, even if the use of low-GWP alternatives should be pursued with a certain urgency.

Hydrocarbons such as propane or isobutane were found to be interesting alternatives to R134a in low-charge systems, such as domestic refrigerators, where the small amount of charge does not lead to flammability problems. Regarding synthetic refrigerants, hydrofluoroolefins (HFOs), R1234yf and R1234ze are interesting options for the substitution of R134a, due to their very low GWP index (equal or even below unity (Sethi et al., 2016)). However, they suffer from other issues, such as mild flammability and insufficient cooling capacity when used as drop-in substitutes. These drawbacks can be partially mitigated by developing new HFO/HFC mixtures, like R450A (R134a and R1234ze (E) blend) and R513A (R134a and R1234yf blend), that are quite interesting as short-term replacement for medium temperature refrigeration and air conditioning systems.

Particularly, R513A is an azeotropic mixture composed of 44/56 mass percentage of R134a/R1234yf, with a zero-Ozone Depletion Potential (ODP) and a GWP value of 573 (Mhyre et al., 2013). Similarly to R134a, R513A is classified as non-flammable fluid (ASHRAE A1), even if it contains per- and polyfluoroalkyl substances (PFAS), that are recently considered as a concern due to their persistence in the environment, potential adverse health effects, and their ability to accumulate in the bodies of living organisms. As regards the thermophysical properties, with respect to R134a, R513A has a lower liquid thermal conductivity (−15%), lower latent heat (−11%) and lower liquid viscosity (−14%), but slightly higher reduced pressure (+15%) and vapor-to-liquid density ratio (+18%). The main characteristics of the two fluids are shown in Table 1, in which the transport and thermodynamic properties are evaluated according to the Refprop 10.1 (Lemmon et al., 2022)

Table 1
Main properties of refrigerants R513A and R134a at 20 °C.

Property	R513A	R134a
ASHRAE Classification	A1	A1
GWP	573	1300
Saturation pressure (bar)	5.81	5.69
Reduced pressure (-)	0.16	0.14
Vapor density (kg/m^3)	30.3	27.7
Vapor-to-liquid density ratio (-)	0.026	0.023
Liquid thermal conductivity (mW/ m K)	72.6	83.3
Liquid viscosity (10^5 Pa s)	18.19	20.77
Prandtl number (-)	3.47	3.50
Latent heat (kJ/kg)	163.6	182.4

database.

According to the state of the art, R513A was mainly experimented for the evaluation of the performance of vapor compression systems rather than to assess its two-phase heat transfer and fluid flow characteristics. As regards the first group of studies, Mota-Babiloni et al. (2017) performed an experimental comparison between R513A and R134a for a mobile air conditioner, and later on for a small size refrigerator (Mota-Babiloni et al., 2018; Makhnatch et al., 2019). In all cases, the authors reported good performances for R513A and better adaptation to the refrigeration system in terms of pressure ratio, discharge temperature and mass flow rate, with respect to both the reference R134a and the other alternative R450A. For domestic refrigerators, the optimal refrigerant charge and the global energy consumption for both R513A and R134a was experimentally evaluated by Yang et al. (2019); Belman-Flores et al. (2022). The first reported that alternative fluid could reduce both by 6% and 3.5%, respectively, and the second obtained similar and more encouraging results (reduction by 17% and 9%, respectively). Finally, Molinaroli et al. (2022) tested R513A in a water-to-water heat pump, obtaining a slight reduction of its cooling capacity (up to 15%) and a COP variation between −2.5% and +3.0% with respect to the employment of the conventional R134a.

As regards instead two-phase thermal and hydraulic experimental studies related to R513A, the literature review presents very few examples. Kedzierski et al. (2018) quantified the pool boiling performance of R513A among other substances on flattened smooth and enhanced surfaces with re-entrant cavities. By imposing a constant wall superheat, the heat flux was found to be 16% lower than that of R134a.

Diani et al. (2020) performed a direct comparison between the thermal performance of a 3.5 mm smooth tube and that of a 3.4 mm microfin tube during R513A condensation under the same working conditions. The authors found, for both cases, a general increase of the condensation heat transfer coefficient with vapor quality and mass velocity. The same tubes were also tested for flow boiling experiments (Diani and Rossetto, 2019), highlighting a strong effect of the mass velocity on the R513A boiling performance, especially for the smooth tube. For the microfin tube, instead, an increased performance up to 300 kg/m^{2}s was found, whereas lower heat transfer coefficients were recorded with further increase of the mass flux.

Finally, the same research group (Diani and Rossetto, 2020) studied flow boiling of R513A in narrower smooth and microfin tubes of 2.5 mm and 2.4 mm, respectively. It was found for the smooth tube that the effect of mass velocity and vapor quality started to be visible for mass velocities higher than 400 kg/m^2 s and at low heat fluxes. For high heat fluxes (60 kW/m^2), instead, the convective behavior was instead never observed. On the other hand, for the microfin tube, the heat transfer coefficients are highly affected by mass velocity and vapor quality, meaning a higher convective contribution due to the presence of the microfins.

As a summary, only few studies are aimed at the investigation of two-phase heat transfer characteristics and are all referred to smooth or microfinned narrow channels, and not to conventional macro-tubes. This research would be useful for the correct design of condensers and evaporators in vapor compression cycles. Therefore, the purpose of the work is to explore thermal and hydraulic characteristics of R513A during flow boiling in a commercial horizontal stainless-steel tube of 6.0 mm internal diameter. The experiments are aimed to evaluate the heat transfer coefficient and the frictional pressure gradient in new operating conditions never explored so far in scientific literature, in terms of mass flux, imposed heat flux, saturation temperature and vapor quality. The thermo-hydraulic performances are then compared with those of R134a in some working conditions. The assessment of the most quoted correlations for both heat transfer and pressure drop is carried out, and a new composite heat transfer prediction method is finally proposed.

2. Test facility and instrumentation

2.1. Experimental set-up and measurement section

The experimental set-up is located at the Refrigeration Laboratory of the Università degli Studi di Napoli Federico II. The same rig was employed for similar flow boiling studies (Arcasi et al., 2022; Arcasi et al., 2021), even if some changes were made in order to help the thermostatic bath handling a higher cooling duty. Fig. 1 illustrates the test facility consisting of two loops: the refrigerant one (depicted by the black line) and the water loop (shown in light blue). The refrigerant, subcooled, is pumped using a magnetic gear pump to a Coriolis mass flow meter to measure its mass flow rate. The fluid then undergoes preheating in a vertical tube using electric heating tapes to achieve saturated conditions and the desired vapor quality. In the test section, both heat transfer coefficient and pressure drop values are assessed. The refrigerant is subsequently condensed in a plate heat exchanger, collected in a liquid vessel, and then subcooled via a tube-in-tube heat exchanger and the pump suction head, effectively closing the main loop. The secondary loop comprises a thermostatic bath and a pump, facilitating the circulation of demineralized water through the subcooler and condenser, which are connected in series. Another tube in tube heat exchanger was added on the secondary loop using tap water to not overload the cooling capacity of the thermostatic bath. Bypass valves can be employed to independently supply either one or both heat exchangers.

The test measurement section comprises a single stainless-steel tube with an internal diameter of 6.0 mm and an outer diameter of 8.0 mm. Fig. 2 shows a picture of the test section without its foam insulating layer. Two pressure ports are positioned at a distance of 237.5 mm for evaluating the inlet pressure and pressure gradient. Additionally, two copper electrodes are placed at a distance of 193.7 mm and welded onto the tube surface to enable tube heating through the Joule effect. The DC current for heating is supplied by a remote-controlled DC power supply unit. To minimize uncertainties in the imposed heat flux and account for electric losses in the line, the real voltage applied to the tube is measured between points C and E in Fig. 2. The test section provides local heat transfer coefficient data at point D. Four T-type thermocouples are placed at the top, bottom, left, and right sections of the tube to measure the outer wall temperature. A thin layer (0.4 mm) of adhesive Kapton ensures electric insulation between the tube and the thermocouples sensing probes. The thermal resistance resulting from the Kapton layer and the epoxy resin used to fix the sensors was determined to be negligible. Detailed geometrical features are presented in Fig. 2.

The measurement instrumentation consists of an array of temperature and pressure transducers positioned along the test facility to ensure accurate system control and management. AC power applied to the preheating section is measured by a wattmeter (accuracy ±1%), and the refrigerant flow rate is determined using a Coriolis mass flow meter (±1%). For the test section heating, the power unit measures the DC current with sufficient accuracy (±1% of the reading), and the DC voltage is obtained through a high-precision analog input module (±0.03%). Calibrated absolute and differential pressure transducers are utilized to assess the refrigerant inlet section (±0.1%) and pressure drop (±0.06 kPa) across the test section. Two RTD resistance thermometers (±0.180 °C) are placed at the test section inlet and outlet to obtain the refrigerant temperature before and after passing through the measurement tube. The 4 T-type thermocouples used for wall temperature measurement exhibit an overall accuracy of ±0.10 °C, achieved through an updated calibration procedure described in the subsequent sections.

3. Method

3.1. Data reduction

The method chosen for the evaluation of the two-phase heat transfer

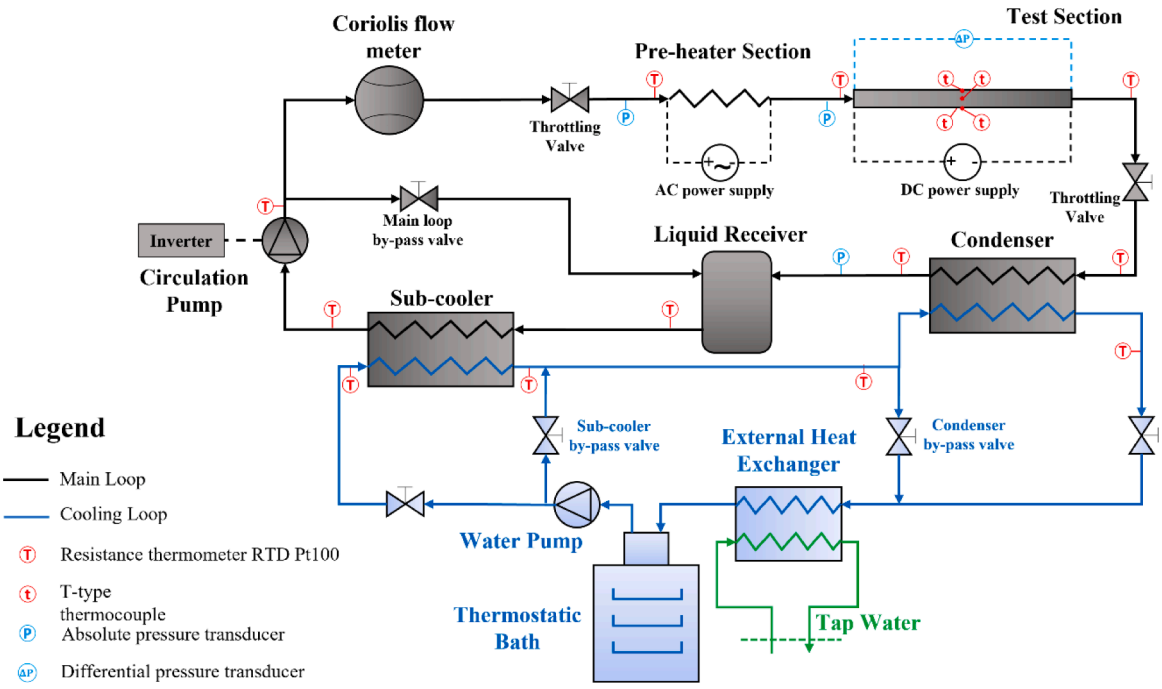

Fig. 1. Schematic of the experimental apparatus.

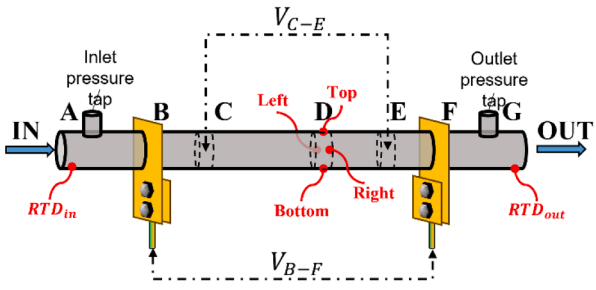

Geometrical features	
AG	237.5 ±0.91 mm
BF	193.7 ±0.79 mm
BD	146.7 ±0.64 mm
CE	101.6 ±0.41 mm
Points Description	
A, G	absolute and differential pressure taps
B, F	copper electrodes
C, E	voltage measurement points
D	HTC measurement point

Fig. 2. Test section characteristics.

coefficient and frictional pressure gradient is typical for flow boiling researches employing electric heating. Particularly, the local heat transfer coefficient was evaluated through Eq. (1), in which the electric heating was assumed to be uniform for the whole section between points B and D (see Fig. 2) and calculated with the measured DC current and voltage.

$$h = \frac{\frac{V_{BD} \cdot I_{tube}}{\pi d \overline{BD}}}{T_{wall,m} - T_{sat,c}} \tag{1}$$

The saturation temperature is linearly determined using temperatures measured by RTDs at the test section inlet and outlet. The mean wall temperature is the average of the four inner wall temperatures (top, bottom, left, and right sides of the tube). The inner wall temperature at each position was calculated assuming 1-D radial heat transfer, uniform heat generation inside the tube, isotropic and homogeneous material, and steady-state conditions. The thermal conductivity used (16.13 W/(m K)) was that of AISI SS316 averaged over typical temperatures in the study. d and D refer to the inner and outer diameters of the test tube, respectively.

$$T_{wall,i} = T_{th,i,out} + \frac{V_{BD} \cdot I_{tube}}{4\pi\lambda_{tube}\overline{BD}} \cdot \frac{\left(\frac{D}{d}\right)^2 \cdot \left(1 - \log\left(\left(\frac{D}{d}\right)^2\right)\right) - 1}{\left(\frac{D}{d}\right)^2 - 1} \tag{2}$$

As regards the calculation of the vapor quality at the measurement point C, it was evaluated as a function of both saturation temperature and local specific enthalpy. Although the studied mixture is almost azeotropic, particular attention was paid to take into account the temperature glide of the mixture in the evaluation of the specific properties in saturated conditions. The dependence on the local specific enthalpy was kept to increase the method accuracy, as also done in our previous publications with non-azeotropic mixtures having a large temperature glide (Mauro et al., 2020; Lillo et al., 2019; Mastrullo et al., 2019).

$$x_c = f\left(T_{sat,c}, i_c\right) \tag{3}$$

The local specific enthalpy was determined using an energy balance over the preheating section and the test section up to the measurement point. The specific enthalpy at the inlet of the preheater depends on temperature and pressure values, both measured immediately before the vertical section of the preheater.

$$i_c = i_{in,preh} + \frac{\dot{Q}_{preh}}{\dot{m}} + \frac{\dot{Q}_{TS}\cdot\left(\frac{\overline{AC}}{\overline{AE}}\right)}{\dot{m}} \quad (4)$$

All the pressure drop values shown in this paper were referred to the only frictional contribution. Since the pressure drop experiments were performed in adiabatic conditions and with a horizontal placement, the momentum and gravitational contributions were not subtracted from the total measured pressure gradient.

$$\left.\frac{\Delta P}{\Delta z}\right|_{fr} = \frac{\Delta P}{\overline{PR}} \quad (5)$$

The data reduction was implemented in MATLAB (2022b) software, and Refprop 10.1 (Lemmon et al., 2022) was used for the evaluation of the transport and thermodynamic properties of the liquid and the vapor phases.

3.2. Experimental procedure

For each experimental run, specific operating parameters such as mass flux, saturation temperature, heat flux, and vapor quality were carefully set to attain a steady-state condition. The user interface's embedded code closely monitors these parameters, issuing a warning if any of them fluctuated beyond a defined threshold. The saturation temperature was adjusted by modifying the thermostatic bath's set-point, while the mass flux was controlled by varying the gear pump's rotational speed or manipulating various throttling and bypass valves in the loop. The desired vapor quality was achieved by adjusting the power of the preheater section, and the heat flux was regulated by controlling the DC power unit's current. For each combination of saturation temperature, mass flux, and heat flux, the experimental heat transfer coefficient was determined by gradually increasing the vapor quality, from the beginning of boiling until post-dryout conditions. Once the steady-state condition was reached, the system was allowed to run for 90 s, during which 90 measurement values were recorded with a frequency of 1 Hz.

3.3. Thermocouple calibration, uncertainty analysis and validation

The 4 T-type thermocouples were calibrated after being placed on the test tube. To achieve this, a series of 80 adiabatic tests were conducted, ranging from 5 °C to 75 °C, covering the entire vapor quality range. Since the temperature of the cold thermocouple junction was unknown, an additional calibrated thermocouple and RTD were positioned in the surrounding environment. For each thermocouple (denoted by i), the function $\Delta T_i = f(\Delta V_i)$ was obtained experimentally. Here, ΔT_i represents the temperature difference between saturated and ambient conditions, and ΔV_i represents the difference in voltage readings between the thermocouple on the tube surface and the one installed in the environment. The combined uncertainty (accounting for instrumental and random fluctuations during experiments) of all parameters was estimated using the law of propagation of error (Moffat, 1985). A coverage factor of 2 was applied to ensure a confidence level greater than 95%. The average uncertainty calculated for all the main parameters of interest during this experimental campaign is presented in Table 2.

Table 2
Average uncertainty recorded for all the parameters of interest.

Parameter	Related uncertainty in stable conditions
Saturation temperature T_{sat}	± 0.16 °C
Mass flux G	±2.25%
Heat flux q	± 0.85%
Vapor quality x	±0.044
Mean heat transfer coefficient h_{mean}	±17.85%
Pressure gradient $\frac{\Delta P}{\Delta z}$	±16.97%

The method validation and verification of all measurement instrumentation were conducted through multiple tests in liquid single-phase conditions. The discrepancies between the imposed heat rate and the calculated one using the energy balance were found to be below 5%. Additionally, the heat transfer coefficients and pressure drops in liquid single-phase flow were measured using the same data reduction procedure as previously described. These results were compared to the predicted values obtained from the Dittus-Boelter correlation (Dittus and Boelter, 1930) for heat transfer and the Blasius friction factor for turbulent flows (Blasius, 1913). The comparison showed good agreement, with differences below 10%.

4. Heat transfer coefficient: results

The experimental campaign comprises approximately 300 tests, covering 30 fixed operating conditions concerning mass flux, saturation temperature, and imposed heat flux. These tests spanned from the onset of boiling to the dry-out and post-dry-out conditions. The working fluid used was R513A, with some tests also repeated using R134a for comparison. Table 3 presents a summary of the imposed working conditions.

4.1. Effect of mass flux, heat flux, saturation temperature and comparison with R134a

Fig. 3a illustrates the effect of mass flux on the mean local heat transfer coefficient. It was observed that the increasing trend with vapor quality represents the heat transfer coefficient behavior for medium-high mass velocities. However, for $G = 150$ kg/m^{2}s, the trend is decreasing, indicating a possible early dry-out or a stratified flow pattern. This assumption is supported by local peripheral values, which indicate a sudden drop in the top heat transfer coefficient just after the onset of boiling. Nonetheless, up to a vapor quality of approximately 0.35, all curves exhibit nearly the same heat transfer coefficient, within the calculated uncertainty range.

In Fig. 3b, the effect of imposed heat flux was demonstrated for a saturation temperature of 50 °C and a mass flux of 500 kg/m^{2}s. It shows that higher heat flux results in a higher mean heat transfer coefficient, with an increase of almost +300% from 10 to 40 kW/m^2. Despite the high mass flux, this behavior suggested that nucleate boiling contribution was significant and was enhanced by the gradual increase of nucleation sites due to the rising imposed heat flux and, consequently, the wall superheat.

Fig. 4a-b presents the effect of saturation temperature for both low and high imposed heat fluxes, focusing on medium-high mass fluxes (non-stratified conditions). For low imposed heat fluxes (Fig. 4a), where the convective contribution plays a major role, increasing the saturation temperature leads to lower heat transfer coefficients, particularly from vapor qualities of 0.40. This reduction results from the higher reduced pressure, which leads to a smaller difference between liquid and vapor phase densities, thereby weakening the slip condition at the interface and affecting convection heat transfer. On the other hand, for high imposed heat fluxes (Fig. 4b), where nucleation is the dominant heat transfer mechanism, a decrease in surface tension results in smaller and more frequent bubbles, promoting the boiling phenomenon and enhancing the average heat transfer coefficient. Similar behavior was

Table 3
Summary of the operating conditions investigated.

Parameter	Range/value
Fluid	R513A
Saturation temperature [°C]	30–50
Mass flux G [kg·m^{-2}·s^{-1}]	150–500
Heat flux q [kW·m^{-2}]	5.0–40
Vapor quality x [-]	0.07 – 0.96
Tube diameter d [mm]	6.0

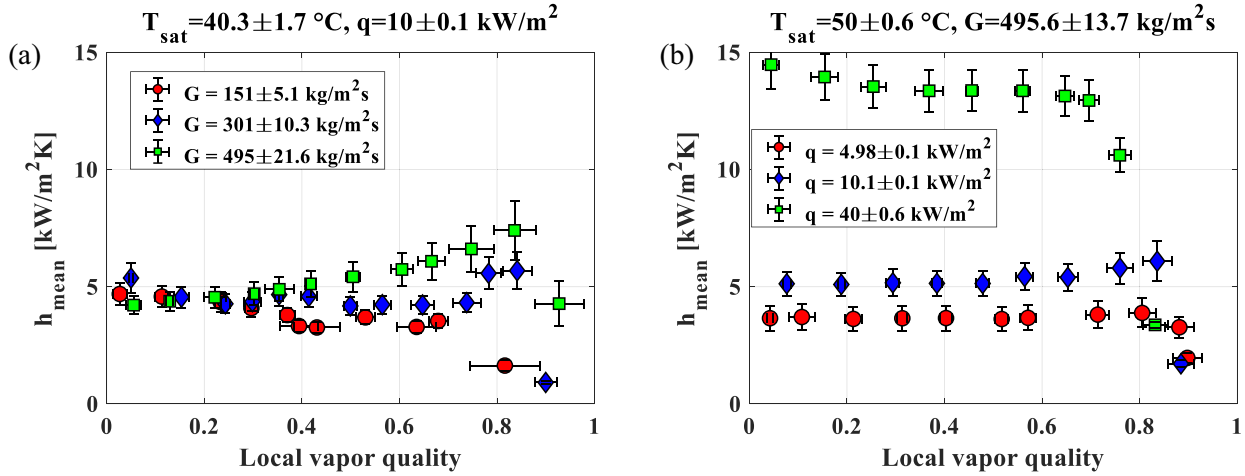

Fig. 3. Mean heat transfer coefficient as a function of the vapor quality, showing the effect of the: (a) mass flux; (b) heat flux, for a fixed saturation temperature.

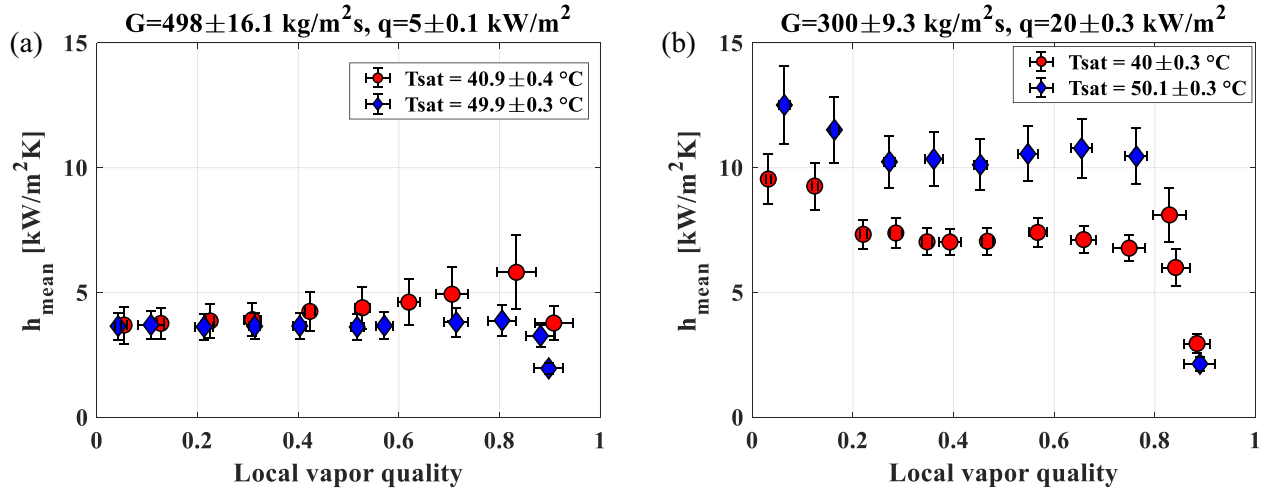

Fig. 4. Mean heat transfer coefficient as a function of the vapor quality, showing the effect of the saturation temperature, for: (a) low imposed heat flux (convective behavior); (b) high imposed heat flux (nucleative behavior).

observed with other fluids (Mastrullo et al., 2018) and in various studies, particularly involving microchannel geometries (Anwar et al., 2014).

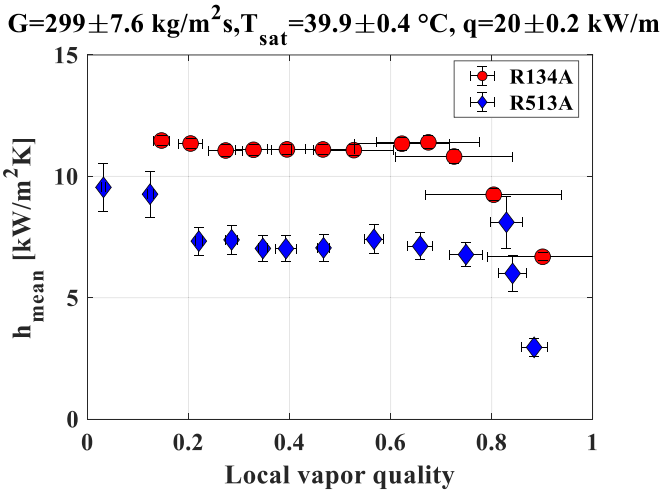

Fig. 5. Mean heat transfer coefficient as a function of the vapor quality for R134a and R513A in the same test tube and sharing the same operating conditions.

Fig. 5 presents the comparison with the reference fluid R134a at a mass flux of 300 kg/m^{2}s, a saturation temperature of 40 °C, and a heat flux of 20 kW/m^2. The heat transfer performance of R134a appeared to be notably higher than that of R513A, spanning from the onset of boiling until the slightly earlier occurrence of dry-out for R134a. These discrepancies could be attributed to the distinct thermophysical and transport properties of the two fluids. Specifically, R134a exhibits a higher latent heat (+15%) and a higher liquid thermal conductivity (+15%), compared to R513A under the same operating conditions.

4.2. *Effect of vapor quality and symmetric/asymmetric local values*

The typical evolution of the local circumferential heat transfer coefficient values at medium-high mass fluxes versus vapor quality is shown in Fig. 6a. For the particular conditions set, namely high mass velocity and low heat flux, the trend with vapor quality was increasing significantly for all the peripheral positions, highlighting the non-negligible convective contribution. It is also evident that the heat transfer coefficient at the top side of the tube is higher than the one measured on the bottom, whereas right and left sides have approximately the same intermediate values. These discrepancies are due to the horizontal tube, that promotes an asymmetric distribution of the liquid film around the wall, leading to lower thermal resistances and therefore higher heat transfer performance where the liquid film is thinner, at

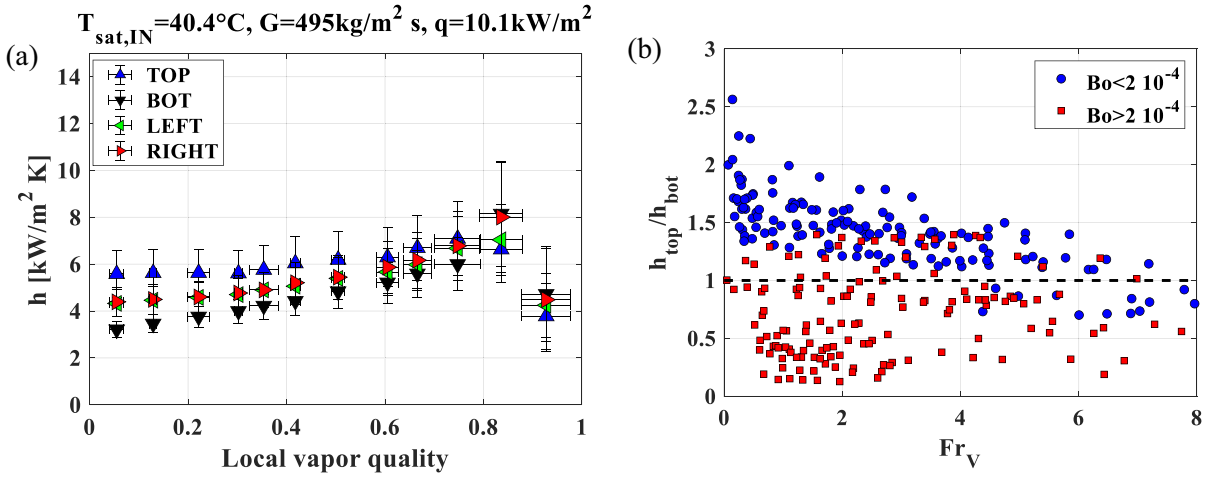

Fig. 6. Asymmetry effect: (a) Local peripheral heat transfer coefficients versus vapor quality; (b) Top-over-bottom heat transfer coefficient ratio as a function of the vapor Froude number, for different boiling numbers.

least up to the dry-out occurrence at approximately $x = 0.85$, in which the liquid no longer wets the top side and the corresponding heat transfer performance drops below those of the other portions of the tube. The asymmetric behavior during annular flow was also observed in our previous publication Lillo et al. (2019), and could be related to the vapor Froude number, as defined in Cioncolini and Thome (2013), and showing the effect of the inertia over the buoyancy forces:

$$Fr_V = \frac{xG}{\sqrt{\rho_V \cdot (\rho_L - \rho_V) g d}} \tag{6}$$

For the present data points, the top-over-bottom heat transfer coefficient ratios are shown in Fig. 6b, divided according to their Boiling number value:

$$Bo = \frac{q}{G \Delta i_{LV}} \tag{7}$$

Experimental data with $Bo > 2\ 10^{-4}$ pertain to low mass fluxes and high imposed heat fluxes, predominantly associated with the nucleate boiling driven heat transfer mechanism or intermittent rewetting of the top surface, indicating partial dry-out. As a consequence, most of these data points exhibit higher bottom heat transfer coefficients compared to their corresponding top values. Conversely, data with $Bo < 2\ 10^{-4}$ mainly relate to symmetric annular flow (at high vapor Froude numbers) or asymmetric annular flow (at low vapor Froude numbers), representing a convective driven heat transfer mechanism.

5. Heat transfer coefficient: assessment of methods and new composite correlation

The R513A heat transfer coefficient data points were compared with predictions from well-known correlations. Table 4 presents the Mean Absolute Percentage Error (MAPE), Mean Relative Percentage Error (MRPE), and the percentage of data points whose error was limited to ±30%, for all the tested methods. None of the selected models satisfactorily predicted the R513A heat transfer coefficient for the entire database. The Gungor and Winterton correlation (Gungor and Winterton, 1986) performed comparatively better with an overall MAPE of 41%, but only 55% of the points fell within a reasonable error band of 30%, as shown in Fig. 7a. Other predictive methods were also assessed but yielded worse outcomes.

Table 4
Assessment of two-phase boiling heat transfer coefficient prediction methods with R513A data.

Correlation	MAPE (%)	MRPE (%)	$\delta_{\pm 30\%}$ (%)
Gungor and Winterton (1986)	40.5	−0.88	55.9
Sun and Mishima (2009)	47.3	+6.72	58.4
Li and Wu (2010)	54.7	+38.1	56.2
Wojtan et al. (2005)	53.9	−5.30	34.2
Bertsch et al. (2009)	65.3	−21.3	28.9
Kim and Mudawar (2013)	72.6	−19.5	24.3
New composite method	25.3	−0.21	74.6

Due to the limited accuracy of the available correlations, a new composite method was here proposed for the calculation of the boiling heat transfer coefficient of refrigerant R513A. Particularly, from the observations of Fig. 6b, the whole database was split in points belonging to convective-driven ($Bo < 2\ 10^{-4}$) and nucleate-driven or partial dry-out ($Bo > 2\ 10^{-4}$) heat transfer mechanism. In the first case, both symmetric and asymmetric annular flow data were satisfactory predicted by the Lillo et al. (2019) approach, as a function of the Froude vapor number and the symmetric heat transfer coefficient h_{C-T} evaluated with the Cioncolini and Thome method (Cioncolini and Thome, 2013) for vertical tubes:

$$h = 1.25 \cdot \left(\frac{0.0789 Fr_V^{1.90}}{1 + 0.0789 Fr_V^{1.90}} \right)^{-0.13} h_{C-T},\ for\ Bo < 2\ 10^{-4} \tag{9}$$

For the remaining database ($Bo > 2\ 10^{-4}$), the best statistic was obtained by using different correlations according to the specific value of the heat transfer coefficient. Particularly, the correlation of Bertsch et al. (2009), Gungor and Winterton (1986), Li and Wu (2010) and Kim and Mudawar (2013) were suggested for the evaluation of the heat transfer coefficient in the following ranges:$h < 2.5$ kW/m^{2}K; $2.5 < h \leq 5.0$ kW/m^{2}K; $5.0 < h \leq 10.0$ kW/m^{2}K; $h > 10$ kW/m^{2}K. The assessment of the present composite method is shown in Fig. 7b.

$$h = h_{Bertsch},\ for\ Bo > 2\ 10^{-4}\ and\ h \leq 2.5\ kW/m^2K \tag{10}$$

$$h = h_{G-W},\ for\ Bo > 2\ 10^{-4}\ and\ 2.5 < h \leq 5.0\ kW/m^2K \tag{11}$$

$$h = h_{Li-Wu},\ for\ Bo > 2\ 10^{-4}\ and\ 5.0 < h \leq 10.0\ kW/m^2K \tag{12}$$

$$h = 1.4 \cdot h_{Kim-Mudawar},\ for\ Bo > 2\ 10^{-4}\ and\ h > 10\ kW/m^2K \tag{13}$$

The complete expression of each correlation is given in the Appendix section. From a practical point of view, a potential user of the correlation for $Bo > 2\ 10^{-4}$ might evaluate the heat transfer coefficient starting from the Bertsch et al. (2009) prediction method and going on with the subsequent models, eventually stopping when the calculated value of h falls in the specified range.

It is worth mentioning, however, that the satisfactory results

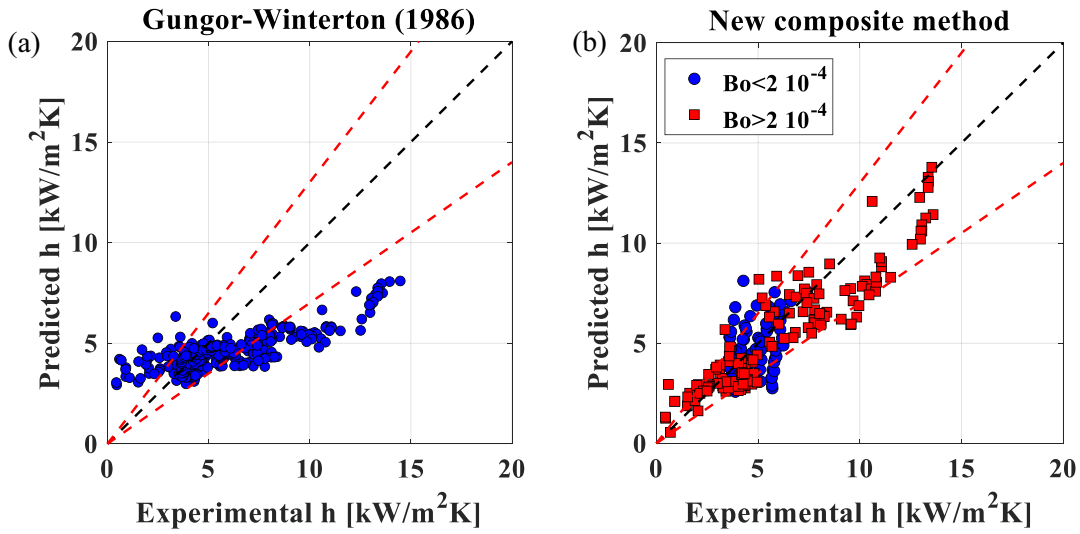

Fig. 7. Experimental versus predicted heat transfer coefficient values according to the new composite method. Points are split according to the boiling number.

obtained with this composite method are intended to be effective in the specific range of operating conditions used for this work and might be influenced by the test tube and its specific features (internal roughness) that would significantly affect the share between nucleate-driven and convective-driven heat transfer.

6. Pressure drop results and assessment of correlations

All the pressure drop results were obtained under the same operating parameters as the heat transfer coefficient tests presented in Table 3, except for the heat flux, which was maintained at zero to ensure an

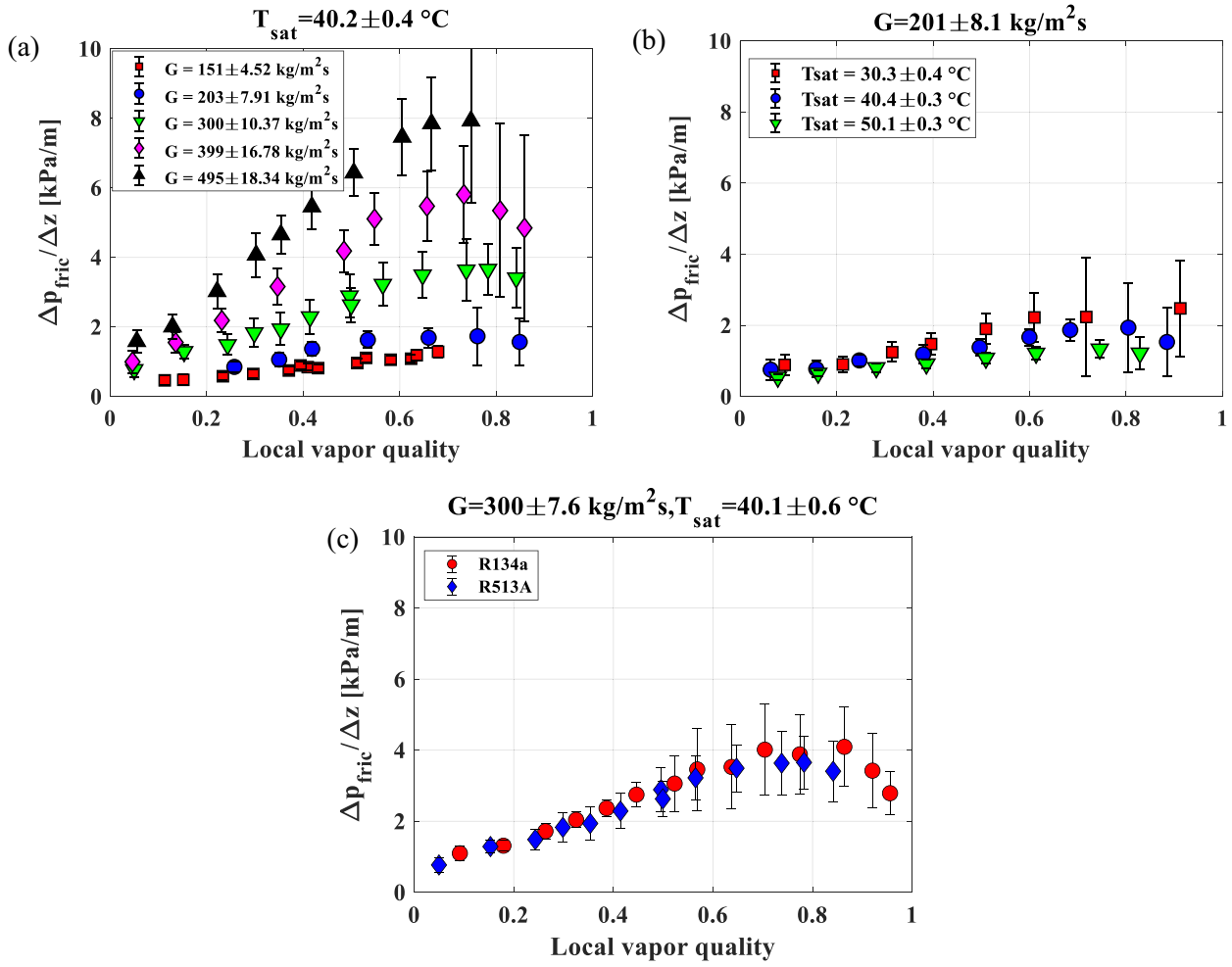

Fig. 8. Frictional pressure gradient as a function of the vapor quality. (a) Effect of the mass flux for R513A; (b) Effect of the saturation temperature for R513A; (c) Comparison between R513A and R134a at the same mass flux and saturation temperature.

adiabatic condition.

The effect of mass flux and saturation temperature is illustrated in Fig. 8a-b. The high uncertainty observed for points with high vapor quality was attributed to significant fluctuations in operating parameters near dry-out conditions. As expected, increasing the mass flux results in higher flow velocities and, consequently, larger frictional pressure gradients, ranging from approximately 1 kPa/m to 8 kPa/m when transitioning from 150 kg/m^{2}s to 500 kg/m^{2}s. In the latter case, the experiment was terminated before dry-out occurrence, as the preheating section supply was insufficient to further increase the vapor quality. With higher saturation temperatures, the frictional pressure gradient decreased due to the higher vapor-to-liquid density ratio near the critical point, leading to a lower slip ratio. When the same operating conditions were applied, R513A exhibited slightly lower pressure drops than R134a, as depicted in Fig. 8c. This discrepancy arose because most of the thermodynamic and transport properties relevant to the friction phenomenon (reduced pressure, densities, and viscosities of the two phases) are nearly identical for both fluids when the same saturation temperature is applied (see Table 1).

The experimental data were compared with well-known predictions from the literature. The complete evaluation, including MAPE, MRPE, and the percentage of data falling within the ±30% error range, is presented in Table 5. The separate flux model of Friedel (1979), based on the liquid-only two-phase multiplier, demonstrated the best accuracy, yielding a MAPE of 13.8% and an MRPE of −3.8%, with 88% of the tests falling within the specified error range. The mechanistic method of Mauro et al. (2022), initially designed for annular flow, also provided satisfactory results for the entire database, with a MAPE of 23.1% and nearly 69% of the data within the ±30% error range. As shown in Fig. 9a, this method provides a sudden change of the frictional pressure gradient, at a vapor quality of approximately 0.60 for the chosen conditions. This is due to the transition from turbulent to laminar flow with the progressive reduction of the liquid film thickness. The Friedel (1979) correlation captured the experimental trend more effectively (see also Fig. 9b), even though it somewhat overpredicted the vapor quality at the pressure drop peak. Among the other prediction methods, the method of Jung et al. (1989) led to significant overpredictions, while the remaining correlations, including the homogeneous models, exhibited lower errors, all underestimating the experimental values.

7. Conclusions

In this study, data on the two-phase heat transfer coefficient during evaporation and adiabatic frictional pressure drop for refrigerant R513A inside a 6.0 mm horizontal stainless-steel tube were collected. The key new findings, experimental trends, correlation assessments, and comparison with the reference fluid R134a are summarized as follows:

- At high mass velocities and low imposed heat fluxes, the heat transfer coefficients exhibited an increasing trend with vapor quality. Local values at the top were generally higher than those at the bottom, suggesting a non-negligible asymmetry in the liquid film thickness at the wall. However, for low mass velocities (tests at $G = 150$ kg/m^{2}s), the decreasing trend with vapor quality indicated the possibility of earlier dry-out and a stratified flow.
- Both convective and nucleate boiling mechanisms contributed to two-phase heat transfer. High mass velocities (>300 kg/m^{2}s) and low heat fluxes (<10 kW/m^2) emphasized convective contributions, while the effect of heat flux was significant, enhancing the heat transfer coefficient by up to +300% as the heat flux increased from 10 kW/m^2 to 40 kW/m^2.
- The effect of saturation temperature depended on the imposed operating conditions. In cases with significant convective contributions, increasing reduced pressure led to a reduction in heat transfer performance. Conversely, when nucleate boiling was the dominant mechanism, the heat transfer coefficient benefitted from higher saturation temperatures.
- None of the tested correlations satisfactorily predicted the heat transfer coefficient, with the Gungor and Winterton (1986) method offering the best accuracy (MAPE = 40%). A new composite method was then developed according to the Boiling number and existing correlations, providing a MAPE of 25.3%.
- Adiabatic frictional pressure gradients increased with higher mass fluxes and lower saturation temperatures. The Friedel (1979) separate flux model could predict 88% of the data within an error range of ±30%, providing a MAPE of 13.8%.
- When compared to the reference fluid R134a at the same operating conditions, R513A exhibited considerably lower heat transfer performance (likely due to its lower liquid thermal conductivity and latent heat) and almost identical frictional pressure gradients (attributed to the very similar viscosities of both fluids).

It is important to highlight that more accurate deductions related to the heat transfer mechanism would require the direct observation of the occurring flow pattern. Also, the declared accuracy of the new composite heat transfer coefficient prediction method is intended only for the specific operating conditions explored by the experimental campaign. More reliable data on this mixture in wider conditions would be useful to extend the validity of the proposed correlation.

Declaration of Competing Interest

The authors declare that they have no known competing financial interests or personal relationships that could have appeared to influence the work reported in this paper.

Appendix

Bertsch et al. (2009) correlation:

$$h_{Bertsch} = h_{Cooper}(1-x) + h_{CB}\left(1 + 80\left(x^2 - x^6\right)e^{-0.6\cdot Co}\right)$$

Table 5
Assessment of two-phase pressure drop prediction methods with R513A data.

Correlation	MAPE (%)	MRPE (%)	$\delta_{\pm 30\%}$ (%)
Friedel (1979)	13.8	−3.8	87.8
Mauro et al. (2022)	23.1	−3.6	68.6
Müller-Steinhagen and Heck, (1986)	27.2	−22.3	66.8
Zhang and Webb (2001)	29.5	−26.3	55.2
Jung et al. (1989)	63.4	+50.9	13.7
Homogeneous Cicchitti et al, (1960)	33.3	−33.1	36.5
Homogeneous Dukler et al. (1964)	48.8	−48.8	5.9
Homogeneous McAdams et al. (1942)	46.8	−46.8	5.9

$$h_{Cooper} = 55\cdot p_{red}^{0.12-0.2\cdot\log_{10}\varepsilon}\cdot\left(-\log_{10}(p_{red})^{-0.55}\right)\cdot M^{-0.5}\cdot q^{0.67}$$

$$h_{CB} = h_{HausenLO}\cdot(1-x) + h_{HausenVO}\cdot x$$

$$h_{Hausen} = \frac{3.66 + 0.0688\cdot Re\cdot Pr\cdot d/L}{1 + 0.04\cdot Re\cdot Pr\cdot d/L}\cdot\frac{\lambda}{d}$$

Gungor and Winterton (1986) correlation:

$$h_{G-W} = E\cdot h_{DB} + S\cdot h_{Cooper}$$

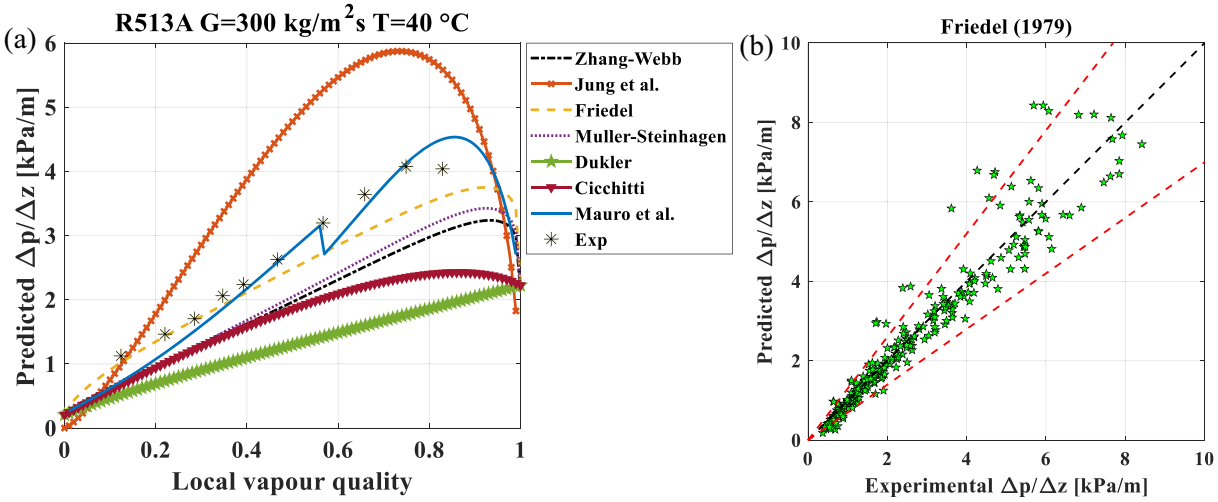

Fig. 9. Assessment of two-phase pressure drop correlations with R513A tests. (a) Trends with vapor quality; (b) Experimental versus predicted values according to the method of Friedel (1979).

$$h_{DB} = 0.023 \cdot Re_L^{0.8} \cdot Pr_L^{0.4} \cdot \lambda_L / d$$

$$E = 1 + 24{,}000 \cdot Bo^{1.16} + 1.37 \cdot \left(\frac{1}{X_{tt}}\right)^{0.86}$$

$$S = \left(1 + 1.15 \cdot 10^{-6} \cdot E^2 \cdot Re_L^{1.17}\right)^{-1}$$

Li and Wu (2010) correlation:

$$h_{Li-Wu} = 334 \cdot Bo^{0.3} \left(Bd \cdot Re_L^{0.36}\right)^{0.4} \cdot \lambda_L / d$$

Kim and Mudawar (2013) correlation:

$$h_{Kim-Mudawar} = \left(h_{NB}^2 + h_{CB}^2\right)^{0.5}$$

$$h_{NB} = 2345 \cdot Bo^{0.7} \cdot p_{red}^{0.38} \cdot (1 - x)^{-0.51} \cdot h_{DB}$$

$$h_{CB} = 5.2 \cdot Bo^{0.08} \cdot We_{LO}^{-0.54} + 3.5 \cdot \left(\frac{1}{X_{tt}}\right)^{0.94} \cdot \left(\frac{\rho_V}{\rho_L}\right)^{0.25} \cdot h_{DB}$$

References

Abas, N., Kalair, A.R., Khan, N., Haider, A., Saleem, Z., Saleem, M.S., 2018. Natural and synthetic refrigerants, global warming: a review. Renew. Sustain. Energy Rev. 90, 557–569.

Anwar, Z., Palm, B., Khodabandeh, R., 2014. Flow boiling heat transfer and dryout characteristics of R152a in a vertical mini-channel. Exp. Therm. Fluid Sci. 53, 207–217.

Arcasi, A., Mastrullo, R., Mauro, A.W., Viscito, L., 2021. Experimental analysis on the hysteresis phenomenon during flow boiling heat transfer in a horizontal stainless-steel tube. Int. J. Heat Mass Transf. 164, 120604.

Arcasi, A., Mauro, A.W., Napoli, G., Viscito, L., 2022. Heat transfer coefficient, pressure drop and dry-out vapor quality of R454C. Flow boiling experiments and assessment of methods. Int. J. Heat Mass Transf. 188, 122599.

Belman-Flores, J.M., Heredia-Aricapa, Y., Pardo-Cely, D., Rodriguez-Valderrama, D.A., De Alba-Rosano, M., Silva-Romero, J.C., 2022. Experimental evaluation of R513A as a low GWP refrigerant to replace R134a in a domestic refrigerator. Int. J. Refrig. 142, 148–155.

Bertsch, S.S., Groll, E.A., Garimella, S.V., 2009. A composite heat transfer correlation for saturated flow boiling in small channels. Int. J. Heat Mass Transf. 52, 2110–2118.

Blasius, P.R.H., 1913. Das aehnlichkeitsgesetz bei reibungsvorgangen in flüssigkeiten. Forschungsheft 131, 1–41.

Choi, S., Oh, J., Hwang, Y., Lee, H., 2017. Life cycle climate performance evaluation (LCCP) on cooling and heating systems in South Korea. Appl. Therm. Eng. 120, 88–98.

A. Cicchitti, C. Lombardi, M. Silvestri, G. Soldaini, R. Zavarettelli, Two-phase cooling experiments: pressure drop, heat transfer and burnout measurements, Energia Nucleare 7 (1960) 407–425.

Cioncolini, A., Thome, J.R., 2013. Liquid film circumferential asymmetry prediction in horizontal annular two-phase flow. Int. J. Multiphase Flow 51, 44–54.

Diani, A., Brunello, P., Rossetto, L., 2020. R513A condensation heat transfer inside tubes: microfin tube vs. smooth tube. Int. J. Heat Mass Transf. 152, 119472.

Diani, A., Rossetto, L., 2019. R513A flow boiling heat transfer inside horizontal smooth tube and microfin tube. Int. J. Refrig. 107, 301–314.

Diani, A., Rossetto, L., 2020. Characteristics of R513A evaporation heat transfer inside small-diameter smooth and microfin tubes. Int. J. Heat Mass Transf. 162, 120402.

Dittus, F.W., Boelter, L.M.K., 1930. Heat transfer in automobile radiators of the tubular type. Univ. Calif. Publ. Eng. 2, 443–461.

Dukler, A.E., Wicks, M., Cleveland, R..., 1964. Pressure drop and hold-up in two-phase flow part A - a comparison of existing correlations and part B - an approach through similarity analysis. AIChE J. 10, 38–43.

Friedel, L., 1979. Improved friction pressure drop correlations for horizontal and vertical two-phase pipe flow. In: Paper E2, European Two Phase Flow Group Meeting. Ispra, Italia.

Gungor, K., Winterton, R., 1986. A general correlation for flow boiling in tubes and annuli. Int. J. Heat Mass Transf. 29, 351–358.

Jung, D.S., McLinden, M., Radermacher, R., Didion, D., 1989. A study of flow boiling heat transfer with refrigerant mixtures. Int. J. Heat Mass Transf. 32, 1751–1764.

Kedzierski, M.A., Lin, L., Kang, D., 2018. Pool boiling of low-global warming potential replacements for R134a on a reentrant cavity surface. J. Heat Transf. 140, 121502.

Kim, S.M., Mudawar, I., 2013. Universal approach to predicting saturated flow boiling heat transfer in mini/micro-channels – part II. Two-phase heat transfer coefficient. Int. J. Heat Mass Transf. 64, 1239–1256.

Lemmon E.W., Mc M.O. Linden, M.L. Huber, REFPROP NIST standard reference database 23, version 10.1; 2022.

Li, W., Wu, Z., 2010. A general criterion for evaporative heat transfer in micro/mini-channels. Int. J. Heat Mass Transf. 53, 1967–1976.

Lillo, G., Mastrullo, R., Mauro, A.W., Pelella, F., Viscito, L., 2019a. Experimental thermal and hydraulic characterization of R448A and comparison with R404A during flow boiling. Appl. Therm. Eng. 161, 114146.
Lillo, G., Mastrullo, R., Mauro, A.W., Viscito, L., 2019b. Flow boiling of R1233zd(E) in a horizontal tube: experiments, assessment and correlation for asymmetric annular flow. Int. J. Heat Mass Transf. 129, 547–561.
Makhnatch, P., Mota-Babiloni, A., Lòpez-Belchì, A., Khodabandeh, R., 2019. R450A and R513A as lower GWP mixtures for high ambient temperature countries: experimental comparison with R134a. Energy 166, 223–235.
Mastrullo, R., Mauro, A.W., Revellin, R., Viscito, L., 2018. Flow boiling heat transfer and pressure drop of pure ethanol (99.8%) in a horizontal stainless steel tube at low reduced pressures. Appl. Therm. Eng. 145, 251–263.
Mastrullo, R., Mauro, A.W., Viscito, L., 2019. flow boiling of R452A: heat transfer data, dry-out characteristics and a correlation. Exp. Therm. Fluid Sci. 105, 247–260.
MATLAB 2022b release. Natick, Massachussets, United States, The MathWorks, Inc.
Mauro, A.W., Napoli, G., Pelella, F., Viscito, L., 2020. Flow boiling heat transfer and pressure drop data of non-azeotropic mixture R455A in a horizontal 6.0 mm stainless-steel tube. Int. J. Refrig. 119, 195–205.
Mauro, A.W., Viscito, L., Revellin, R., 2022. Void fraction and pressure gradient model for an adiabatic symmetric annular developed flow with entrainment. Int. J. Multiphase Flow 153, 104126.
McAdams, W., Woods, W., Bryan, R., 1942. Vaporization inside horizontal tubes-ii-benzene-oil-mixtures. J. Heat Transf. 64, 193–200.
Mhyre, G., Shindell, D., Bréon, F.M., Collins, W., Fuglestvedt, J., Huang, J., 2013. Anthropogenic and natural radiative forcing. In: climate change 2013: the physical science basis, Contribution of WGI to the Fifth Assessment Report of the Intergovernmental Panel on Climate Change. Cambridge University Press, Cambridge, United Kingdom and New York, NY, USA.
Moffat, R.J., 1985. Using uncertainty analysis in the planning of an experiment. Trans. ASME: J. Fluids Eng. 107, 173–178.
Molinaroli, L., Lucchini, A., Colombo, L.P.M., 2022. Drop-in analysis of R450A and R513A as low-GWP alternatives to R134a in a water-to-water heat pump. Int. J. Refrig. 135, 139–147.
Mota-Babiloni, A., Belman-Flores, J.M., Makhnatch, P., Navarro-Esbrì, J., Barroso-Maldonado, J.M., 2018. Experimental exergy analysis of R513A to replace R134a in a small capacity refrigeration system. Energy 162, 99–110.
Mota-Babiloni, A., Makhnatch, P., Khodabandeh, R., Navarro-Esbrì, J., 2017. Experimental assessment of R134a and its lower GWP alternative R513A. Int. J. Refrig. 74, 682–688.
Müller Steinhagen, H., Heck, K., 1986. A simple friction pressure drop correlation for two-phase flow in pipes. Chem. Eng. Process.: Process Intensif. 20, 297–308.
Pelella, F., Viscito, L., Mauro, A.W., 2022. Soft faults in residential heat pumps: possibility of evaluation via on-field measurements and related degradation of performance. Energy Convers. Manag. 260, 115646.
Ritchie, H., Roser, M., 2020. CO_2 and Greenhouse Gas Emissions. Published online at OurWorldInData.orgRetrieved from. https://ourworldindata.org/co2-and-other-greenhouse-gas-emissions.
Sethi, A., Becerra, E.Vera, Motta, S.Yana, 2016. Low GWP R134a replacements for small refrigeration (plug-in) applications. Int. J. Refrig. 66, 64–72.
Stocker, T.F., 2013. Contribution of Working Group I to the Fift Assessment Report of the Intergovernmental Panel On Climate Change. Cambridge University Press, Cambridge.
Sun, L., Mishima, K., 2009. An evaluation of prediction methods for saturated flow boiling heat transfer in mini-channels. Int. J. Heat Mass Transf. 52, 5323–5329.
The European Parliament and the Council of the European Union, 2014. Regulation (EU) No 517/2014 of the European Parliament and the Council of 16 April 2014 on fluorinated greenhouse gases and repealing Regulation (EC) No 842/2006. Off. J. Eur. Union 150, 195–230.
Wojtan, L., Ursenbacher, T., Thome, J.R., 2005. Investigation of flow boiling in horizontal tubes: part II - developement of a new heat transfer model for stratified-wavy, dryout and mist flow regimes. Int. J. Heat Mass Transf. 48, 2970–2985.
Yang, M., Zhang, H., Meng, Z., Qin, Y., 2019. Experimental study on R1234yf/R134a mixture (R513A) as R134a replacement in a domestic refrigerator. Appl. Therm. Eng. 146, 540–547.
Zhang, M., Webb, R.L., 2001. Correlation of two-phase friction for refrigerants in small-diameter tubes. Exp. Therm. Fluid Sci. 25, 131–139.